Available online at www.eccomasproceedia.org
Eccomas Proceedia SMART (2023) 549-559

ECCOMAS
Proceedia

X ECCOMAS Thematic Conference on Smart Structures and Materials
SMART 2023
D.A. Saravanos, A. Benjeddou, N. Chrysochoidis and T. Theodosiou (Eds)

A COMPARISON BETWEEN TWO DIFFERENT LAYOUTS OF ADAPTIVE TUNED MASS DAMPER BASED ON SHAPE MEMORY ALLOYS

S. MANZONI[*], A. ARGENTINO[*], M. BERARDENGO[**], F. LUCA'[*] AND M. VANALI[†]

[*] Department of Mechanical Engineering
Politecnico di Milano
Milan, Italy
e-mail: stefano.manzoni@polimi.it

[**]Department of Mechanical, Energy, Management and Transportation Engineering
Università degli Studi di Genova
Genoa, Italy

[†]Department of Engineering and Architecture
Università degli Studi di Parma
Parma, Italy

Abstract. Tuned mass dampers (TMD) are well-known devices used to attenuate vibrations in primary systems, from small to large size. To be effective, TMD dynamic features (i.e., eigenfrequencies and non-dimensional damping ratios) must be properly tuned on those of the primary system. This in turn implies that when a mistuning occurs, due to, e.g., temperature shifts, the vibration reduction performance worsens. To avoid this, different studies have been devoted to develop adaptive TMDs able to change their dynamic features to recover the tuned condition. Among the different possible approaches, the use of shape memory alloys (SMA) is gaining more and more attention in the field of adaptive TMDs. This is because their special features allow developing effective and reliable adaptive TMDs capable to change their eigenfrequency when the SMA elements are heated/cooled.

This paper is aimed at comparing the two main layouts of SMA-based adaptive TMDs: one is based on a cantilever beam of SMA material, while the other relies on a pre-strained SMA wire with a central oscillating mass. The comparison is carried out in terms of adaptation capability, force exerted on the primary system and electrical power consumption. The comparison is carried out by means of models of the adaptive TMDs, validated through experiments.

Key words: tuned mass damper, adaptive tuned mass damper, shape memory alloy, vibration, damping

Peer-review under responsibility of the organizing committee of SMART 2023.
doi: 10.7712/150123.9809.445295

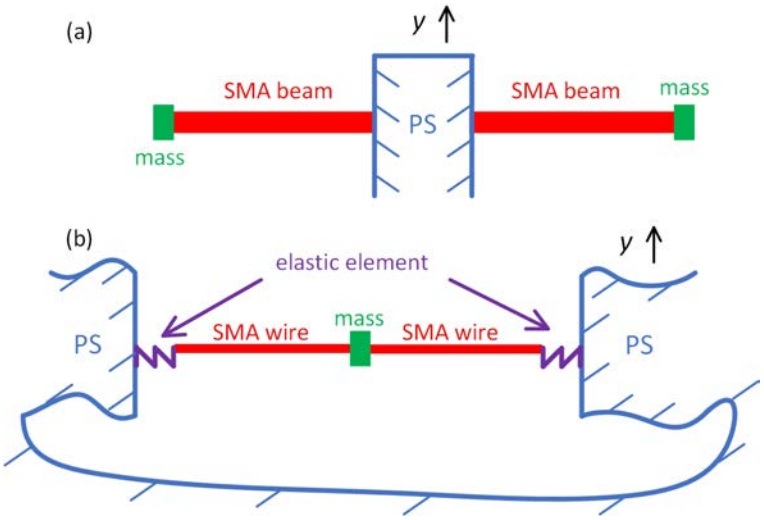

Figure 1: Layouts of the SMA-based ATMDs: beam-based (a) and wire-based (b). PS means primary system.

1 INTRODUCTION

Tuned mass dampers (TMD) are well-known devices for lowering vibrations of primary systems/structures (e.g., [1, 2]). Once their dynamic features are properly tuned on those of the primary system, they are usually able to significantly lower the vibrations of the primary system itself. The main issue related to the use of TMDs is that when a mistuning occurs (e.g., due to environmental changes) the vibration reduction worsens. To avoid such a situation, many researchers are developing adaptive tuned mass dampers (ATMD) which are devices able to change their dynamic features (e.g., [3, 4]) in response to an external stimulus. This allows for recovering the perfect tuning in cases where an initial mistuning occurs.

Different principles can be used to build ATMDs (e.g., [5, 6]) and the development of devices based on shape memory alloys (SMA) is very promising. The two main layouts of SMA-based ATMDs are cantilever beams (e.g., [7, 8]) and wires with a central mass (e.g., [9]) (which can be also used for multi-mode control by adding further masses [10]); see Fig. 1. It is noticed that the layout based on the beam is here considered using two beams (see Fig. 1a) in order to have only a force acting on the primary system, thus avoiding any torque. In both cases, changing the electrical current flowing through the SMA elements, they are heated/cooled.

Although both the layouts are able to provide significant vibration reductions, few works in the literature compared them. This comparison, which is the main aim of this paper, will be carried out in terms of:

- adaptation capability which indicates how much the ATMD eigenfrequency can be changed. It is noticed that, for damping adaptation, both the ATMD layouts can be easily coupled to similar additional devices such as, e.g., eddy current devices [9];
- force exerted by the ATMD on the primary system/structure, that is related to the achiev-

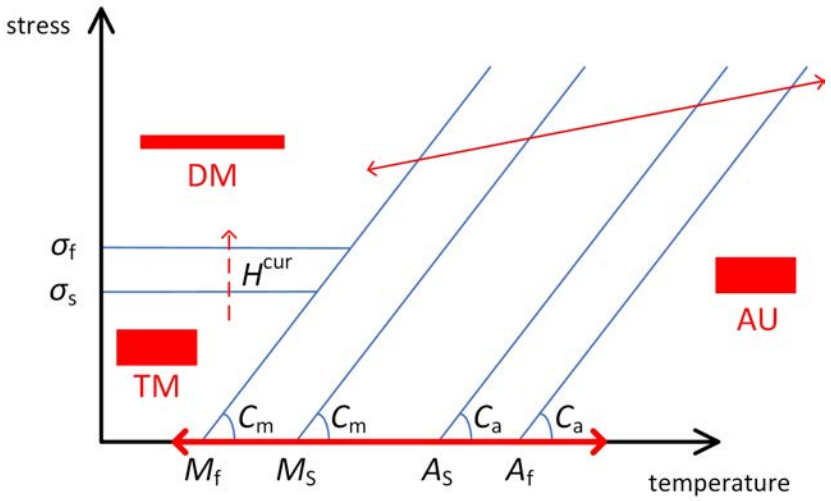

Figure 2: Temperature-stress plot for SMA elements.

able attenuation performance;

- power consumption related to the need of having electrical current flowing through the SMA elements in order to make the TMD adaptive.

The paper is structured as follows: Section 2 briefly describes the working principle and how to model the ATMDs, Section 3 presents an experimental campaign performed to show the effectiveness of the two ATMDs and, finally, Section 4 compares the two ATMD layouts by using the mentioned models.

2 ATMD WORKING PRINCIPLE AND MODEL

This section explains the working principles and how to model the two ATMDs in order to be able to link the value of the input current i to the obtained frequency response function of the ATMD. Section 2.1 discusses the beam-based ATMD, while 2.2 presents the the wire-based ATMD.

2.1 Beam-based ATMD

Considering the typical temperature-stress diagram of SMA elements (see [9, 11] for more details), the working principle for this ATMD can be described as follows: it is possible to pass from Twinned Martensite (TM) to Austenite (AU) and vice versa by changing the temperature at null stress (see the thick red solid double arrow in Fig. 2). Since the SMA material has the same shape in AU and TM, the main change in the SMA element during the mentioned transformation is related to the Young's modulus. This principle is used to build SMA cantilever beams, whose eigenfrequency is changed by changing the temperature T of the beam.

The model of this ATMD relies on three different sub-models which are then gathered to link the input current i to the frequency response function (FRF) of the ATMD.

The first model is a thermal model which allows finding the relationship between the current i provided to the SMA-beam and its resulting temperature T. Then, the material model allows deriving the link between T and the values of the properties of the SMA material (e.g., the Young's modulus). Finally, a dynamic model links these properties to the FRF of the ATMD. More in detail, the FRFs considered are those between the primary system displacement Y at the contact point and the displacement W of a given point of the beam (named G_{WY}) and between Y and the force S exerted by the ATMD on the primary system (named G_{SY}).

Gathering all the three sub-models, a global model describing the link between the imposed i and the FRFs is obtained. Details about these models are available in [12].

2.2 Wire-based ATMD

Another way to have a phase transformation in the SMA material is to apply a stress over σ_{f} and then change temperature to pass from detwinned martensite (DM) to AU and vice versa, as evidenced by the thin red solid double arrow in Fig. 2 (see [11, 12] for more details). This double arrow does not mean that the temperature–stress states experienced by the SMA element are the same in both the directions of transformation, but only that, changing temperature, also a change of stress occurs. The eigenfrequency change is mainly related to the change of shape (between AU and DM), even if also a change of the material parameters occurs. Relying on this principle, it possible to build an ATMD by means of an oscillating SMA wire with a central mass. The SMA wire is pre-stressed over σ_{f} by employing elastic elements (see Fig. 1b) which also connect the SMA wire to the primary system. The temperature variation is obtained by changing the value of the electrical current that is made flow through the SMA wire.

Also in this case, three sub-models (i.e., thermal, material and dynamical) are gathered to find the final link between the imposed i and the previously mentioned FRFs. In this case, the global model results more complicated compared to that of the beam-based ATMD because of the change of shape and stress of the wire during the transformations. The detailed description of all the models is provided in [12].

3 EXPERIMENTAL VALIDATION OF THE ATMDS

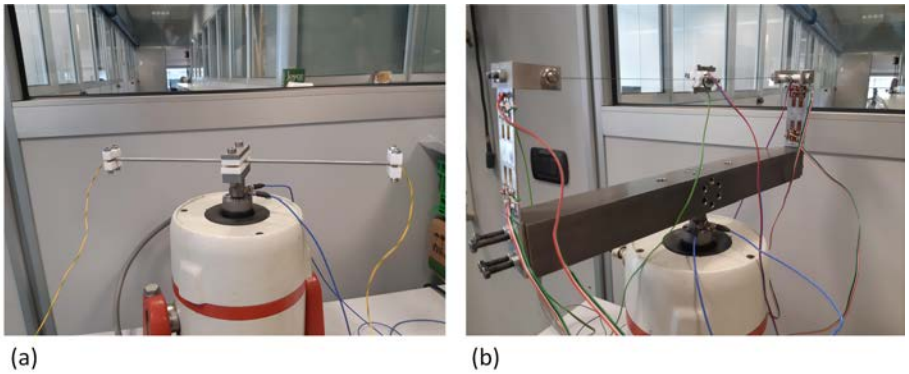

Figure 3: Experimental set-ups: beam-based ATMD (a) and wire-based ATMD (b).

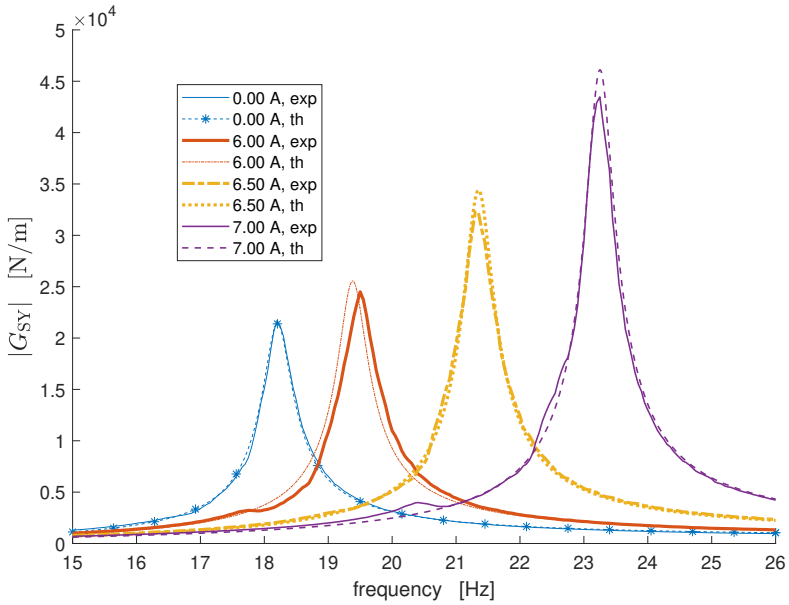

Figure 4: Experimental and theoretical amplitudes of FRFs G_{SY} for the beam-based ATMD while heating.

This section presents some tests to the aim of showing the reliability of the mentioned models and to give further evidence to the working principles of the ATMDs. The set-ups used are presented in Fig. 3 (see also [12]).

Figure 4 shows that there is a good fit between experimental and model FRFs for the beam-based ATMDs (similar results have been obtained for the wire-based ATMD); see [12]. More

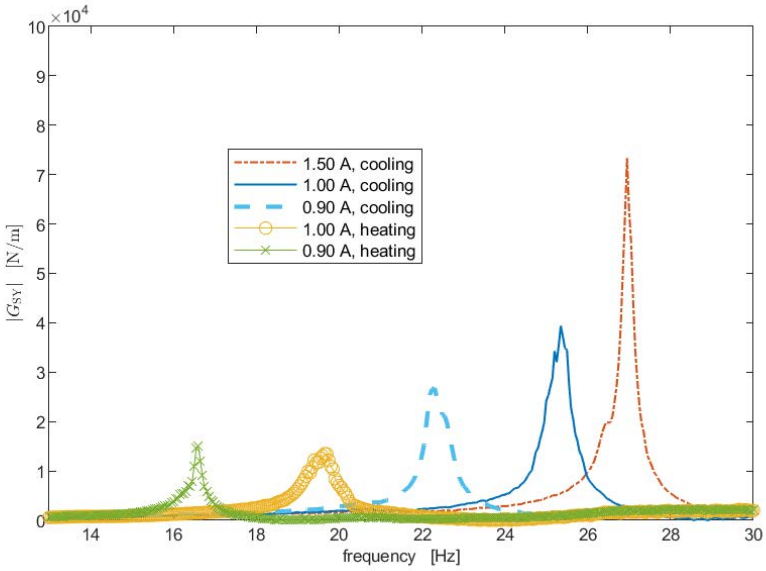

Figure 5: Experimental amplitudes of FRFs G_{SY} for the wire-based ATMD while either heating or cooling the SMA wire.

in detail, the figure presents the FRFs between Y and S for different values of the input current i.

For both the ATMDs, it is observed that a higher eigenfrequency value can be obtained with a lower temperature (and, thus, a lower input current i) when cooling compared to heating (see Fig. 5 for the wire-ATMD, as an example). This is due to the fact that the threshold temperatures related to the start of the transformation from TM/DM to AU are larger compared to the corresponding ones of the transformation from AU to TM/DM (see Fig. 2). More details and results about all these tests are available in [12].

4 COMPARISON OF THE ATMD LAYOUTS

This section presents the comparisons between the two different layouts of ATMDs. The nominal data used for the comparison are presented in Table 1. Section 4.1 discusses the comparison in terms of adaptation capability, Section 4.2 compares the two ATMDs in terms of force exerted on the primary system and, finally, Section 4.3 performs the comparison in terms of electric power consumption. In all the cases, the two ATMDs are designed such that they show the first eigenfrequency ω_1 equal to 30π rad/s at environmental temperature (i.e., when a null current i is supplied). Furthermore, the global mass M_{tot} of the two ATMDs is kept equal in all the comparisons in order to have the same weight for the two devices under analysis. The mass M_{tot} is the sum of the mass of the wire/beam plus the additional concentrated masses (see Fig. 1). To perform the comparisons, the following data have been assumed: wire with a circular cross-section with diameter of 0.5 mm and beam with circular hollow section with outer diameter of 4 mm and thickness of 0.5 mm; furthermore, the non-dimensional damping

Table 1: Parameter values for both SMA beams and wires used for the comparisons. See [12] for the definition of all the symbols.

Parameter	Value
A_s [°C]	68.6
A_f [°C]	78.9
M_s [°C]	55.2
M_f [°C]	42.7
C_A [MPa/°C]	9.90
C_M [MPa/°C]	6.83
H^cur [-]	$4.39{\cdot}10^{-2}$
α [°C^{-1}]	10^{-6}
E_m [GPa]	32.1
E_a [GPa]	39.5
ρ_m [Ωm]	$90{\cdot}10^{-8}$
ρ_a [Ωm]	$100{\cdot}10^{-8}$

ratio for the considered resonances of the ATMDs was set equal to 1%, and the stiffness of the elastic elements for the wire layout (see Fig. 1b) was set in order to have a stress value equal to 50 MPa in DM at environmental temperature and 200 MPa in AU. More details and results about all these comparisons are available in [12].

4.1 Adaptation capability

When a sufficient current i is supplied to bring the SMA elements in AU phase, the change of eigenfrequency of the wire-based ATMD is approximately ten times larger than for the beam-based ATMD. This result is mostly the same for all the considered values of M_tot (i.e., between 0.02 and 0.30 kg).

4.2 Force exerted on the primary system

The starting point for this comparison is the eigenfrequency range covered by the beam-based ATMD. According to the previous sub-section, it is the layout with the narrower range of frequency adaptation, varying from $\omega_1^{\mathrm{M,beam}}$ to $\omega_1^{\mathrm{A,beam}}$ (the superscript M indicates that the SMA element is in martensite at environmental temperature, while the superscript A indicates that the SMA element has been heated such that the AU phase has been reached). The wire-based ATMD can be tuned correspondingly as described here below.

The wire is tuned such that $\omega_1^{\mathrm{M,wire}} = \omega_1^{\mathrm{M,beam}}$=30$\pi$ rad/s (i.e., 15 Hz) at environmental temperature (point 1 in Fig. 6a). Then, the temperature T of the wire is increased until complete AU transformation is obtained. Being $\omega_1^{\mathrm{A,wire}} > \omega_1^{\mathrm{A,beam}}$, the temperature of the wire is then decreased. The temperature decrease is stopped when $\omega_1^{\mathrm{wire}} = \omega_1^{\mathrm{A,beam}}$ (point 2 in Fig. 6a). The

frequency value results equal to approximately 33.28π rad/s (i.e., 16.64 Hz). The comparison of the two ATMD layouts is thus carried out at 15 (see points 1 in Figs. 6a and b) and 16.64 Hz (see points 2 in Figs. 6a and b).

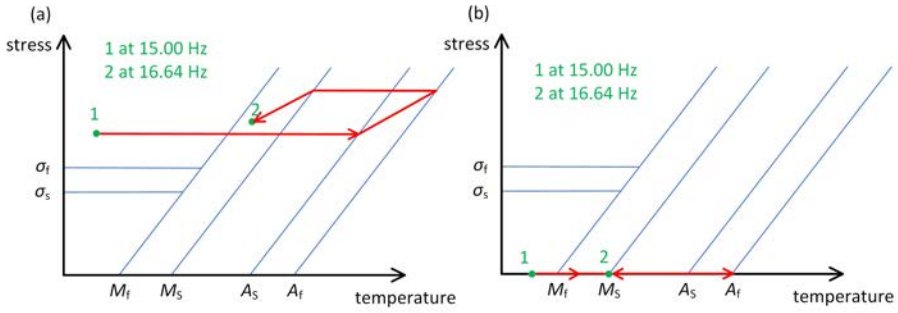

Figure 6: Heating/cooling paths considered for the comparisons: wire-based ATMD (a) and beam-based ATMD (b).

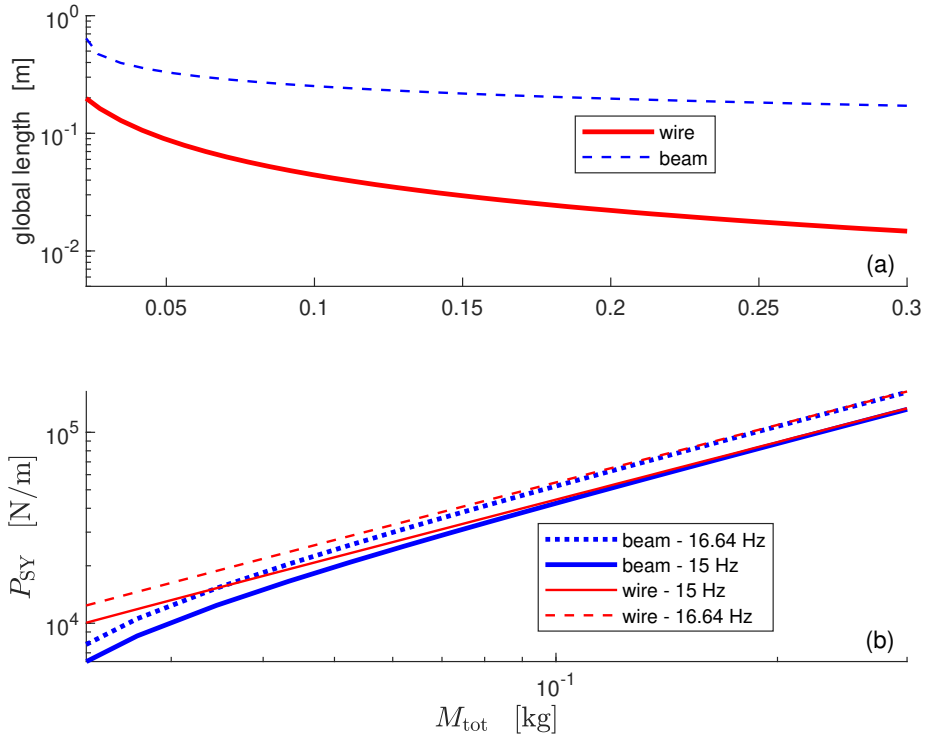

Figure 7: Trends of ATMD global length (a) and P_{tot} (b) as functions of M_{tot}.

First of all, the relationship between M_{tot} and the corresponding global length at environ-

mental temperature of the ATMD is presented in Fig. 7a. It emerges that the wire-based layout results shorter compared to the beam-like ATMD. Figure 7b shows the peak values of the FRF between Y and S (i.e., the values at resonance), named P_{SY}. As expected from the experimental results, the mentioned peaks are higher at higher frequency (compare the curves related to different frequency values in the same plot). Wire- and beam-based ATMDs provide similar forces, when the M_{tot} value increases, while higher forces are produced by the wire-based ATMD for low values of M_{tot}.

4.3 Electric power consumption

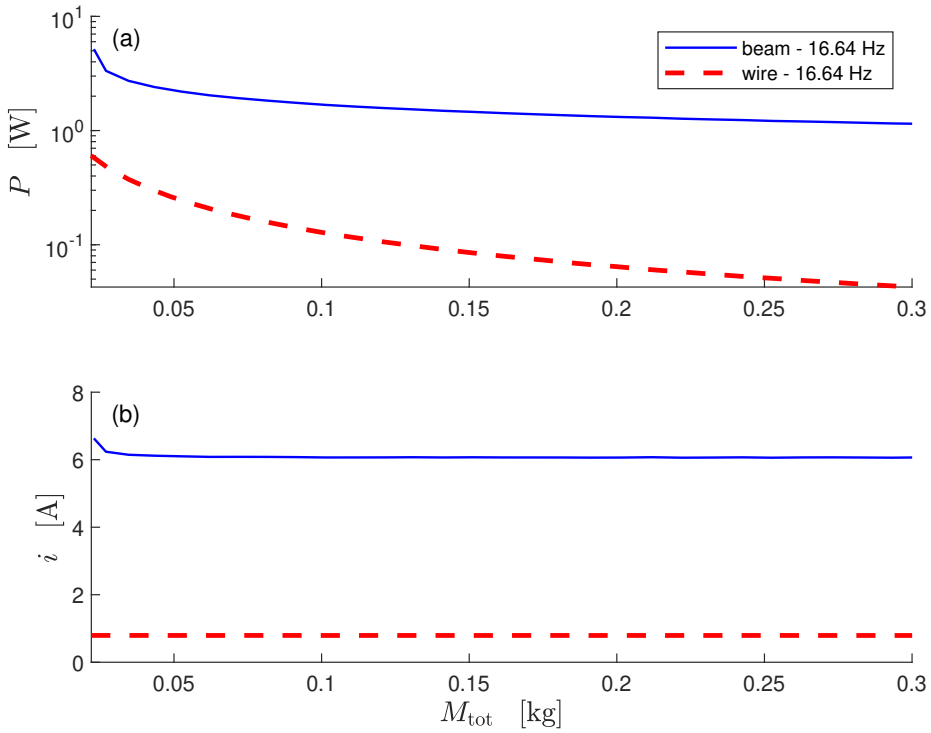

Figure 8: Trends of P (a) and i (b) as functions of M_{tot}.

This comparison is performed in terms of power P and current i needed to bring the ATMD at the maximum eigenfrequency value (i.e., 16.64 Hz in this case).

Figures 8a and b show the power P and the current i, respectively, as a function of M_{tot}. Addressing the comparison between wire- and beam-ATMD, the former results much less expensive in terms of electrical consumption. Often, the power consumption required by the wire-ATMD is approximately ten times lower than that of the beam-ATMD.

5 Conclusion

The paper has dealt with the comparison of two SMA-based ATMD layouts: beam-based and wire-based. This comparison has been carried out by means of models describing the relation between the current made flow through the SMA elements and the dynamics of the ATMD. The models have also been validated through experiments. The wire-based layout shows better performances but its design is more complicated.

REFERENCES

[1] S. Krenk and J. Høgsberg, "Equal modal damping design for a family of resonant vibration control formats," *Journal of Applied Mechanics*, vol. 19, no. 9, pp. 1294–1315, 2013.

[2] F. Santos and J. Nunes, "Toward an adaptive vibration absorber using shape-memory alloys, for civil engineering applications," *Journal of Intelligent Material Systems and Structures*, vol. 29, no. 5, pp. 729–740, 2018.

[3] L. Zhang, L. Hong, J. S. Dhupia, S. Johnson, Z. Qaiser, and Z. Zhou, "A novel semi-active tuned mass damper with a continuously tunable stiffness," *Proceedings of the Institution of Mechanical Engineers, Part C: Journal of Mechanical Engineering Science*, vol. 237, pp. 281–293, 2023.

[4] L. Wang, S. Nagarajaiah, Y. Zhou, and W. Shi, "Experimental study on adaptive-passive tuned mass damper with variable stiffness for vertical human-induced vibration control," *Engineering Structures*, vol. 280, 2023.

[5] F. Weber and M. Maślanka, "Frequency and damping adaptation of a TMD with controlled MR damper," *Smart Materials and Structures*, vol. 21, no. 5, p. 055011, 2012.

[6] G. M. Chatziathanasiou, N. A. Chrysochoidis, C. S. Rekatsinas, and D. A. Saravanos, "A semi-active shunted piezoelectric tuned-mass-damper for multi-modal vibration control of large flexible structures," *Journal of Sound and Vibration*, vol. 537, p. 117222, 2022.

[7] E. Rustighi, M. J. Brennan, and B. R. Mace, "A shape memory alloy adaptive tuned vibration absorber: design and implementation," *Smart Materials and Structures*, vol. 14, no. 1, pp. 19–28, 2005.

[8] K. Williams, G. Chiu, and R. Bernhard, "Adaptive-Passive Absorbers Using Shape-Memory Alloys," *Journal of Sound and Vibration*, vol. 249, no. 5, pp. 835–848, 2002.

[9] M. Berardengo, A. Cigada, F. Guanziroli, and S. Manzoni, "Modelling and control of an adaptive tuned mass damper based on shape memory alloys and eddy currents," *Journal of Sound and Vibration*, vol. 349, pp. 18–38, 2015.

[10] M. Berardengo, G. Della Porta, S. Manzoni, and M. Vanali, "A multi-modal adaptive tuned mass damper based on shape memory alloys," *Journal of Intelligent Material Systems and Structures*, vol. 30, no. 4, pp. 536–555, 2019.

[11] D. Lagoudas, *Shape memory alloys: modeling and engineering applications*. Springer, 2008.

[12] S. Manzoni, A. Argentino, F. Lucà, M. Berardengo, and M. Vanali, "Sma-based adaptive tuned mass dampers: Analysis and comparison," *Mechanical Systems and Signal Processing*, vol. 186, 2023.